Article

Bacterial Cellulose and Biodegradable Superbase for Heterogeneous Transesterification to Alkyl Esters

Cristina Ionela Gogoaşă [1,2], Cristian Eugen Răducanu [1,*], Laura Elisabeta Petraş [1,3], Doiniţa Roxana Cioroiu Tîrpan [4], Gabriel Vasilievici [5], Andreea Luiza Mîrţ [5], Tănase Dobre [1,6] and Oana Cristina Pârvulescu [1]

[1] Chemical and Biochemical Engineering Department, National University of Science and Technology POLITEHNICA Bucharest, 1-7 Gheorghe Polizu St., 011061 Bucharest, Romania; cristina_ionela_92@yahoo.com (C.I.G.); laurapetras@yahoo.ro (L.E.P.); tghdobre@gmail.com (T.D.); oana.parvulescu@yahoo.com (O.C.P.)

[2] Laropharm, 145 A Alexandriei St., Bragadiru, 077025 Ilfov, Romania

[3] Petromidia, 215 Navodari Blvd., 900527 Constanta, Romania

[4] Department of Chemistry and Chemical Engineering, Ovidius University of Constanta, 124 Mamaia Blvd., 900527 Constanta, Romania; tirpanroxana@gmail.com

[5] National Institute for Research Development for Chemistry and Petrochemistry-ICECHIM, 202 Spl. Independentei, S6, 060021 Bucharest, Romania; gvasilievici@icechim.ro (G.V.); luiza.mirt@icechim.ro (A.L.M.)

[6] Technical Sciences Academy of Romania, 26 Dacia Blvd., 030167 Bucharest, Romania

* Correspondence: cristianrdcn1@yahoo.com

Abstract: Heterogeneous catalysts, basic, acidic or bifunctional, can catalyze transesterification reactions where the raw material has a significant content of FFA fatty acids, such as used cooking oils or other lipid-based residues, which do not have the purity required for homogeneous catalysis, in which case the purity of the triglycerides above 99.5% is the first condition for the initiation of the reaction, to avoid saponification. In this work, a green supported catalyst was developed, using bacterial cellulose as catalytic support and biodegradable superbase as a chemical compound, for transesterification reaction to obtain alkyl esters, yielding over 99% of its content at 70 °C temperature and 7.5% catalyst loading (1.5/20 *w/w* catalyst:oil). A Plackett—Burman design was used for screening experiments to explore the main effect in terms of catalytic activity and performance of the triglyceride conversion reaction.

Keywords: bacterial cellulose; heterogeneous catalyst; superbases; transesterification; Plackett–Burman design; methyl esters

1. Introduction

Biofuels should be non-disputable alternatives to fossil fuels, as biofuel technologies already scaled up, or in pilot phase (involving production of biodiesel, bioethanol or biogas) are waiting to be integrated in the fuel matrix of any economy, lowering the pressure on its energy system.

Considering the multiple disadvantages of the production, refining, and use of fossil fuels, starting with their depletion, or the environmental problems due to CO_2 emissions, one can instead resort to technologies for the production of biofuels or synthetic fuels, which can be produced as much as necessary, benefiting from the knowledge of the last 15–20 years of new techniques and technologies [1], gaining in the end its own energy dependence, fuels or otherwise.

Regarding the insertion of biofuels into the fuel matrix of the economy, it should be noted that, for several years, solutions have also started to come from the large companies producing petro-fuels, and two directions are worth mentioning; the first would be the one where they comply with the biofuel content regulations at the gas station pump, ranging from 6 to 10% ethanol (E6/E10) or B6/B10, while the second is the solution

they proposed in regarding awareness of climate change issues, namely hydrotreating or hydroprocessing [2–5], the option that some oil companies are considering to address, or even commercially produce, so-called green diesel.

Hydroprocessing of vegetable oils involves hydrodeoxygenation of triglycerides and hydrorefining of derived products in the presence of catalysts and H_2 environment. This type of process leads to obtaining mixtures and liquid hydrocarbons (HC), usually *n*-paraffins C15–C18, with a boiling point below that specific to fossil diesel, which are also called green diesel or bio-dehydrogenated diesel. In most cases, the hydrodeoxygenation process takes place on $Ni/Co/Mo-Al_2O_3$-type catalysts or other proprietary patented catalysts [2] to obtain long chains of n-paraffins, while the hydro-isomerization step is carried out by using specific, specially designed catalysts to obtain specific cold flow properties by converting *n*-paraffins to *iso*-paraffins. This hydro-isomerization is the most critical stage because obtaining the flow properties for the produced green diesel must not compromise the cetane number or other properties required for its use in aviation, for example.

This technology is already applied commercially [5] and, among the existing solutions, we also find the possibility of retrofitting in the case of some industrial platforms with installations for fossil fuels. The implementation of these operations does not require additional installations and can be easily integrated into the infrastructure of some refineries, with several companies expressing their interest in this green diesel production technology.

Biofuels are, on the other hand, chemical compounds of synthesis. Homogeneously catalyzed commercial biodiesel is an excellent choice, therefore, to complement fossil fuel (or even replace it in some cases, e.g., agriculture operation involving diesel engine machinery, interurban merchandise transport, or in areas of temperate continental clime). This process converts, mostly, fresh soy, sun flower, or rapeseed oil (considered though conflictual raw material [6]) to the final main product, alkyl esters. Improvements have been made in the last years regarding safety or environmental consideration [7]. Still, alkyl esters producing technologies can also sustain changes, in terms of raw material nonconflictual destination, reduced stage number of the process, which contributes further to minimizing several process costs, and even a better control of end-process waste waters. Such changes may involve using lipid wastes of all kinds, from waste cooking oils, animal factory waste, or municipal waste; basically, every waste containing lipid can be transformed into a transesterification raw material process, all of them conditioned by its availability as raw material (feedstock process) for production capacity ranging between 20,000 t/year for local, small communities and up to 100–1,000,000 t/year, similar to those of fossil fuel.

Although mature as a technology, the commercial production of biodiesel could still undergo another injection of new techniques, such as that of heterogeneous catalysis, which is insufficiently widespread but can be helpful in increasing biodiesel production, based on long-term and precise strategies on a certain (broad) economy market segment—agriculture, transport, and residential heating—and depending on how much this biofuel can replace or supplement fossil fuel. The transition to the second (or third) generation of biofuel will only complete this circle of green solutions offered for this in climate change issues [8].

A different technique can also be approached in terms of transesterification catalysis, particularly in heterogeneous base catalysts [9], able to transform such second-generation-type raw materials and able to yield 98% conversion at alcohol:oil (25:1), catalyst loading (1.5% *w/v*), and temperature 65 °C [9]; ~98.5% biodiesel using methanol: oil molar ratio of 9:1 in 1.5 h reaction time at 65 °C reaction temperature of catalyst loading of 10 wt.% (to oil) [10]; or 98% fatty acids methyl esters content for 2.5 wt.% catalyst loading and 1:9 oil:methanol molar ratio at 65 °C reaction temperature [11]. Other advantages of this approach are the ease of separation of the final product, the ability to build a heterogeneous catalyst adapted to a certain type of waste raw material, and perhaps cost reductions, obtained from the first two [10,11]. If the heterogeneous catalyst is built from a catalytic support and combined with a compound (basic in our case), the key lies in choosing a specific type of catalytic support from many others (there are a multitude of options), compatible with the basic or acid catalyst, it being rather difficult to find an exact fit for these two components.

Among this multitude of suitable materials capable of being transformed into a catalytic support, bacterial cellulose (BC) has the versatility required for this type of approach, if considered as a catalytic support.

As can be found in many studies, the versatility of BC is special. The characteristics of the cellulosic matrix or the absence of hemicellulose [12] provide multiple options in functionalization strategies. The use of BC falls into many fields, with just as many applications. Applications in the biomedical field can be developed around the characteristics and properties of BC [13,14] and can go from the construction and use as a material biocompatible with human tissue, respectively, in different forms of treatments [15] up to the drug carrier, helping to transport it [16].

Due to the inclusive improvement of BC production methods, whether it is about its production in a static medium or especially if a mobile medium is used [17], the applications for which BC can be used, based on its mechanical properties as well as special ones that can help it incorporate classic materials, include the textile industry or the leather industry [17]. Different membranes can be obtained by functionalizing BC membranes or are capable of permeation or simple filtration [18–20].

The functionalization strategy of BC membranes can include at least two different approaches, the first being the use of this membrane after the post-production treatment process and after total dehydration and the second involves membrane pre-drying treatments, aiming to replace water molecules with functional molecules, capable of easily binding to compounds with the required properties [21]. In this context, a heterogeneous green catalyst was developed in this work, within the concept of green chemistry, in terms of environmentally friendly, nontoxic, and highly biodegradable nonconflictual materials, by using the newly produced solid material as a matrix to combine it with a superbase also having green chemistry characteristics and used to heterogeneously catalyze transesterification reactions, yielding over 99% methyl ester content, while a Plackett–Burman design was used for screening experiments to explore the main effect in terms of catalytic activity and triglyceride conversion reaction performance.

2. Results and Discussion

2.1. Scanning Electron Microscope (SEM) Analysis of Heterogeneous Catalyst and Catalytic Support

The surface morphology study for the bacterial cellulose membranes was performed using scanning electron spectroscopy (SEM) for each type of material stu. Figure 1 shows images for a membrane (simple, nontreated BC) surface with morphological characteristics often found in similar studies: a cellulose fibrillar network, yet unaltered (Figure 1c), with whole fibers intercrossed, in short, a typical BC surface morphology.

Figure 2 shows images of BC_{Gu} membrane with slight structural changes ((Figure 2b,d)—very slight modification if compared with the images for plain BC from Figure 1c with images from Figure 2a,c) and nanocrystals starting to aggregate on the membrane surface.

Visible morphological changes of catalyst $BC_{Gu-4K24\,h}$ can be observed in SEM images in Figure 3a compared to both the surface non-altered by alkalinity of BC shown in Figure 1c and the slightly modified BC surface morphology shown in Figure 2.

The shape of the 3D nanocrystals can be observed, different from that noticed in Figure 2c, whose formation may be due to the reaction product between the two strong bases. It should also be noted that the heterogeneous catalyst shown in Figure 3 (SEM image of its surface) was kept for 24 h after the impregnation reaction in a 4K BC_{Gu-K} solution because, compared to the surface morphology of the BC_{Gu} catalyst, significant changes in the dispersion of basic aggregates on its surface are easy to spot, introducing us to a first variable to follow when developing the strategy of combining the two, catalyst and catalytic support.

A similar approach can be discussed after comparing Figures 4 and 5 with Figure 6, in terms of adsorption capacity vs. adsorption time strategy, which is probably time-dependent in this impregnation reaction. The catalyst loading is more visible on the BC

surface shown in the SEM image of Figure 5 with a functionalization time of 24 h than on the BC surface in the SEM image of Figure 4, where, although the functionalization time is 96 h, the BC was treated in 8 K solution, while the BC in the SEM image of Figure 6 shows the highest presence of superbase nanocrystals dispersed on the BC surface.
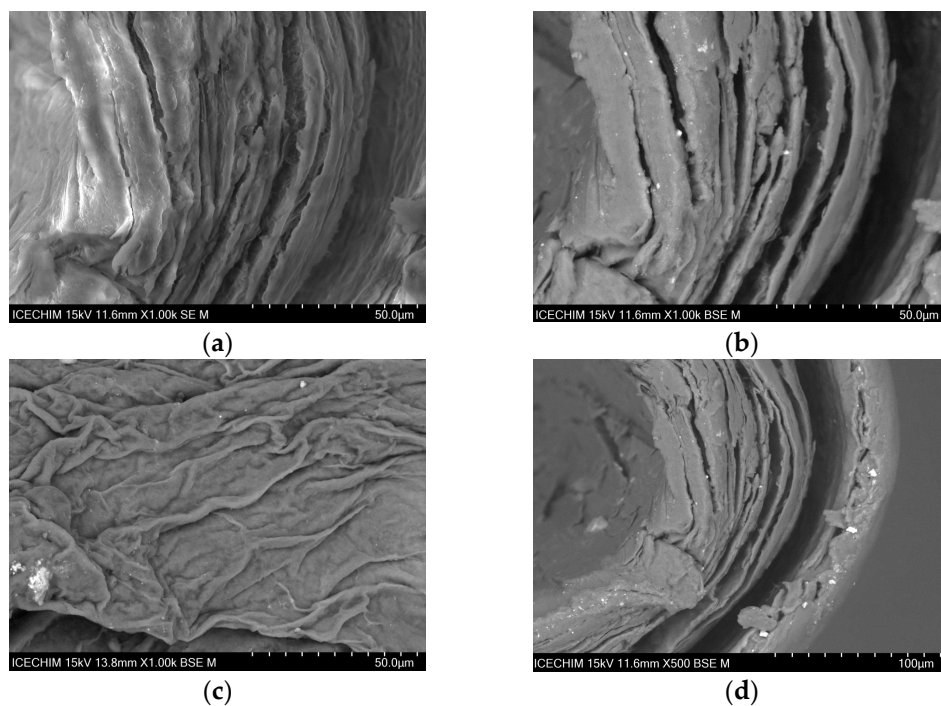

Figure 1. SEM image of catalytic support (*BC*) before functionalization, common *Acetobacter* sp. strain specific surface: (**a**,**b**,**d**) pore network (channels); (**c**) membrane surface with visible cellulosic network fibrils.
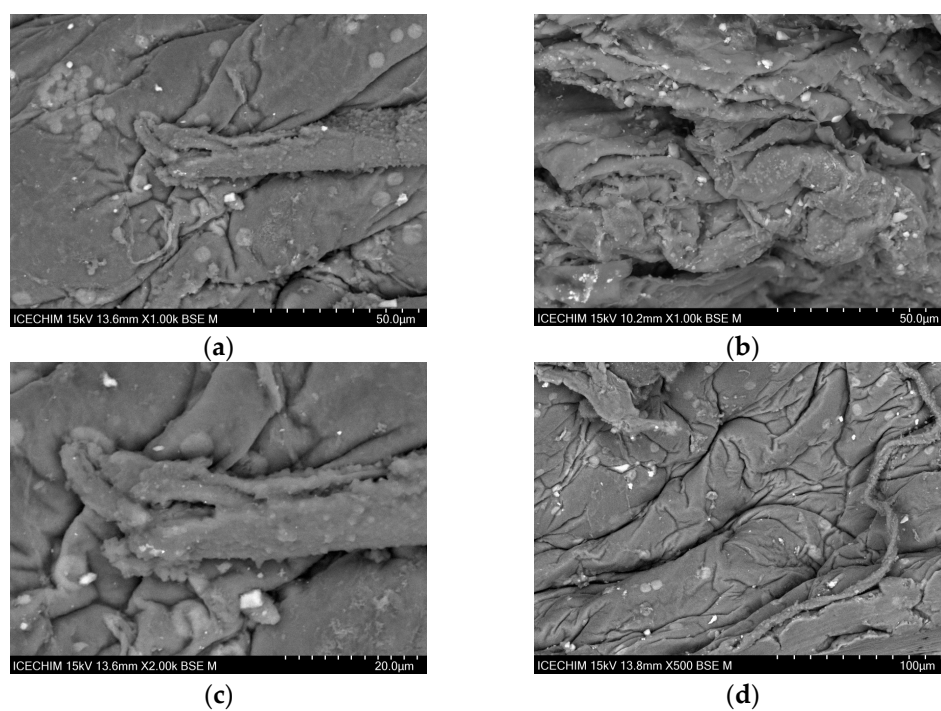

Figure 2. SEM catalytic support (*BC*$_{Gu}$) after functionalization in guanidine alcoholic solution: (**a**,**c**,**d**) loaded/dispersed guanidine nanocrystals; (**b**) membrane surface altered by alkalinity.
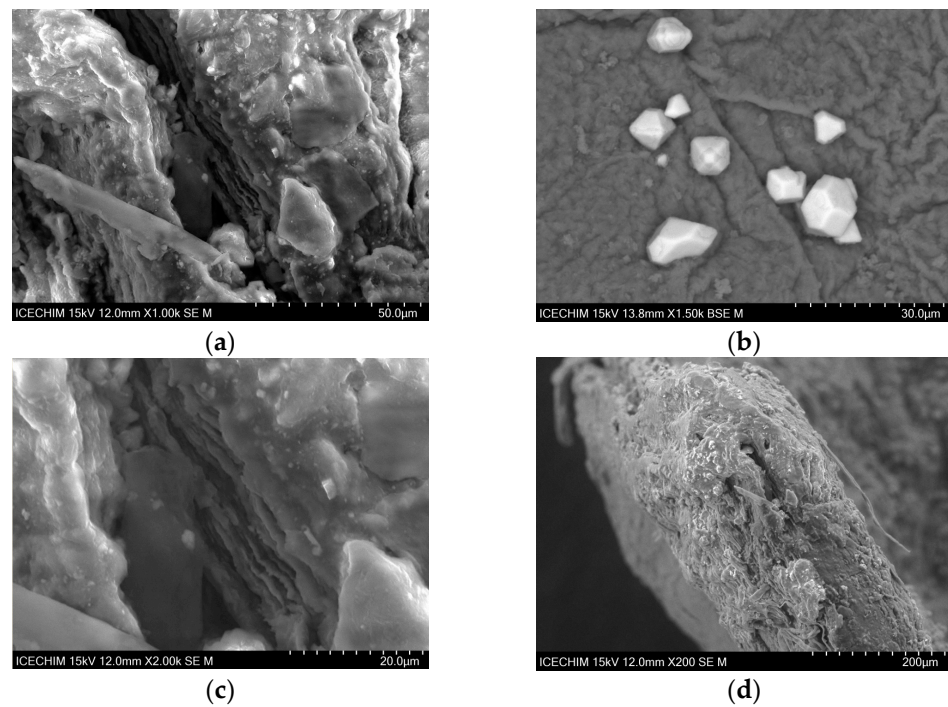
Figure 3. SEM image of catalyst ($BC_{Gu\text{-}4K24\,h}$): (**a**,**b**) microcrystals of alkaline compound dispersed; (**c**) altered surface, newly formed pore channel; (**d**) intercalated catalyst and fibrillar cellulose.
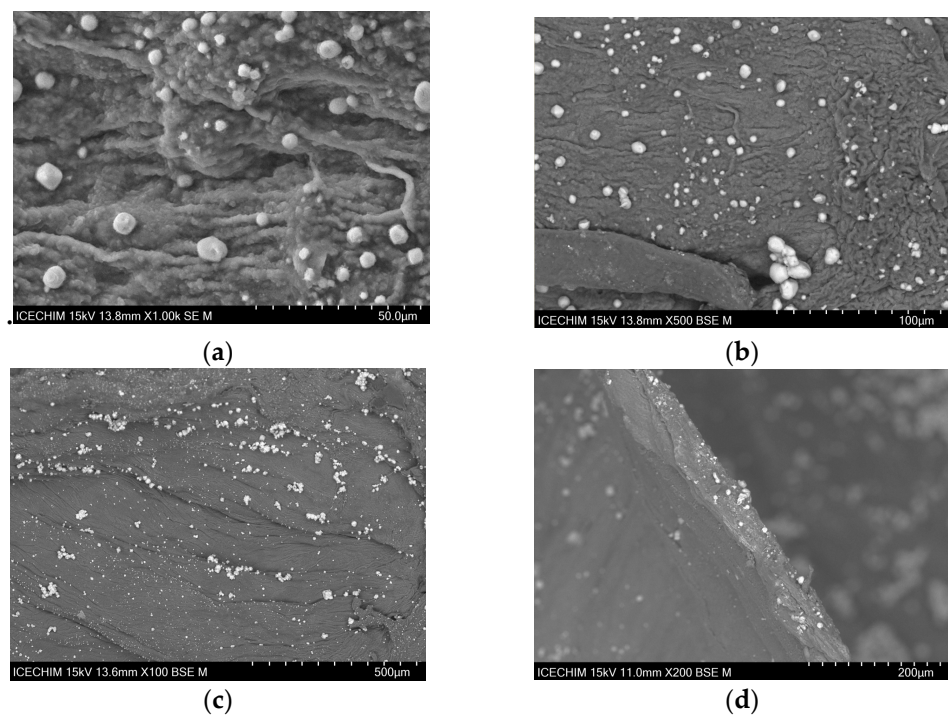
Figure 4. SEM image of catalyst ($BC_{Gu\text{-}4K96\,h}$): nanoparticle aggregation due to higher impregnation time (**b**,**c**); (**a**,**d**) improved distribution on the surface due to a possible better adsorption.
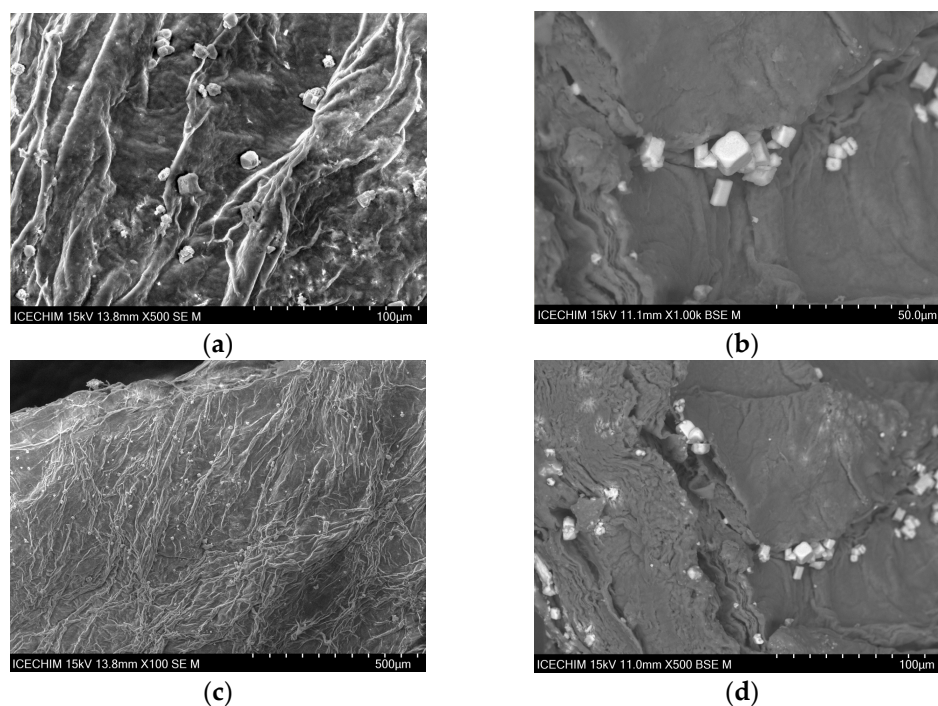
Figure 5. SEM image of catalyst ($BC_{Gu-8K24\,h}$): (**a**,**c**) fibrillar network (intercrossed) and nanoparticle-wrapped; (**b**,**d**) pores acting as sites for basic nanoparticle aggregates.
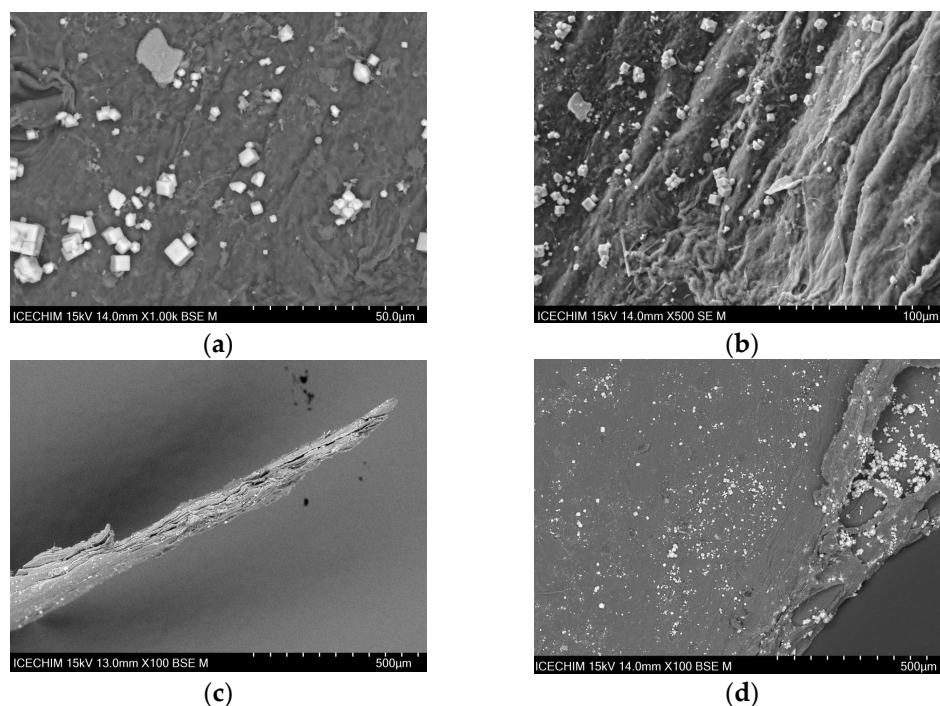

Figure 6. SEM image of catalyst ($BC_{Gu-8K96\,h}$): (**a**,**b**) highly visible 3D shape of basic nanocrystals (**b**,**c**); (**c**,**d**) enhanced distribution on the surface due to higher nanoparticle adsorption.

2.2. Fourier Transform Infrared Spectroscopy for Heterogeneous Catalyst and Catalytic Support

FT-IR analysis was conducted to evaluate potential interactions and functional groups present both in the nonfunctionalized BC materials and the treated BC (basic heterogeneous catalyst). Figure 7 shows the characteristic peaks of a simple BC membrane, similar to those found in the literature data, common to the membranes produced by different strains [22–24], in a range of 4000–400 cm^{-1}, and OH groups at the wavelength of 3342 cm^{-1} can be

observed due to its stretching vibrations and C–H bonds at 2899 cm^{-1} wavelength band due to stretching vibration of aliphatic C–H bonds.
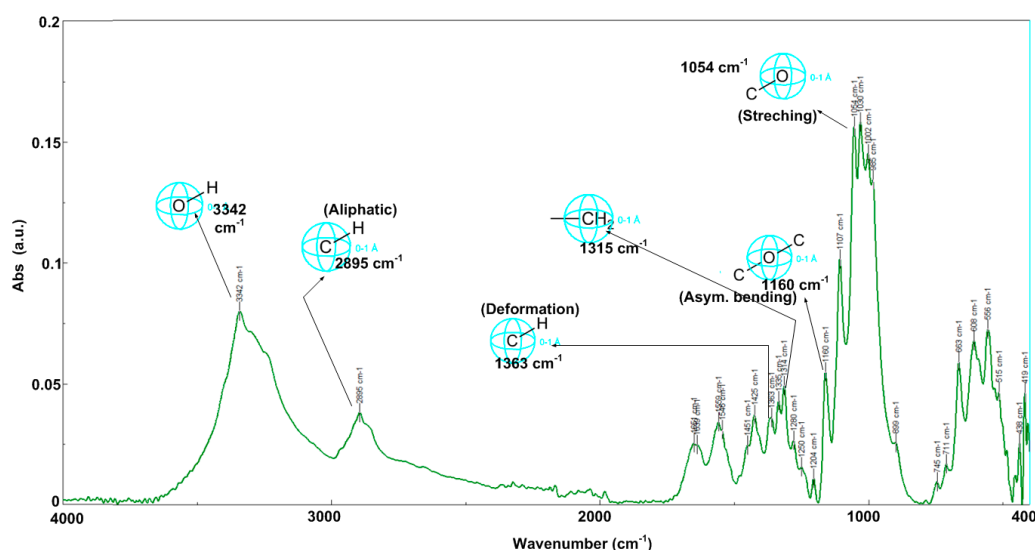

Figure 7. FT-IR spectra of simple BC: particular potential functional groups specific to a simple BC membrane from *Acetobacter* sp. strain.

Characteristic peaks can also be observed at wavelength 1054 cm^{-1}, which can be attributed to C–O bond stretching; at 1365.35 cm^{-1} wavelengths and 1432 cm^{-1}, which can be attributed to C–H deformation; and at 1432 cm^{-1} wavelength for potential C–H symmetric bending, [22–24] while peaks at 1159 cm^{-1} can be attributed to asymmetric bending of the C–O–C bonds [22–24].

Figures 8 and 9 show new peaks following the functionalization of BC of potential N–H bonds, characteristic at wavelength bands of 3230–3285 cm^{-1} from the stretching vibration of N–H groups, linked to guanidinium cations [23], as well as the characteristic peaks for potential C–N bonds at 1368−1370 cm^{-1} from the hydrogen bond vibration [23], as expected to be influenced by guanidine treatment.

Figure 8. FT-IR spectra of BC from *Acetobacter* sp. strain: functional groups specific to functionalization with guanidine/potassium hydroxide (BC_{Gu-4K}).
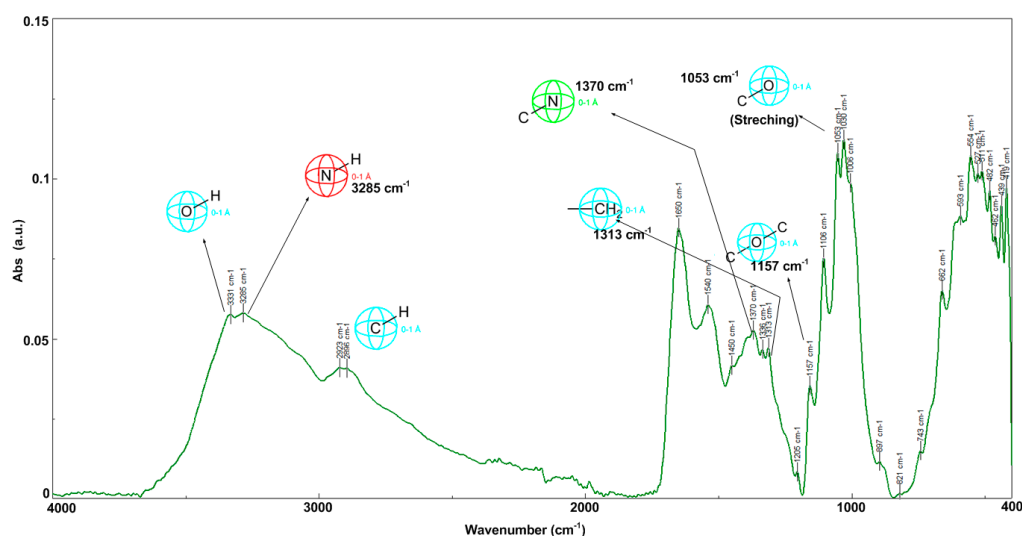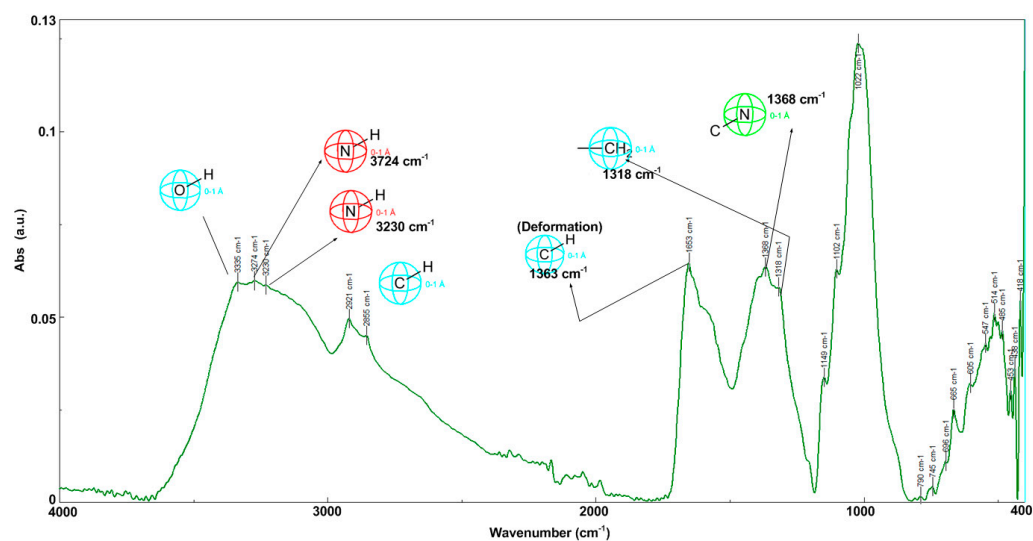
Figure 9. FT-IR spectra of BC from *Acetobacter* sp. strain: functional groups specific to functionalization with guanidine/potassium hydroxide ($BC_{Gu\text{-}8K}$).

Figure 10 summarizes the evaluation of potential chemical bonds and functional groups, before and after the preparation of the catalyst, allowing us to observe how the chemical bonds potentially formed on the bare catalytic support were affected by the superbase impregnation by weakening the hydrogen bonds, allowing the development of new ones but with the intended characteristics in terms of strong basicity due to both the amino- and imino-functional group.
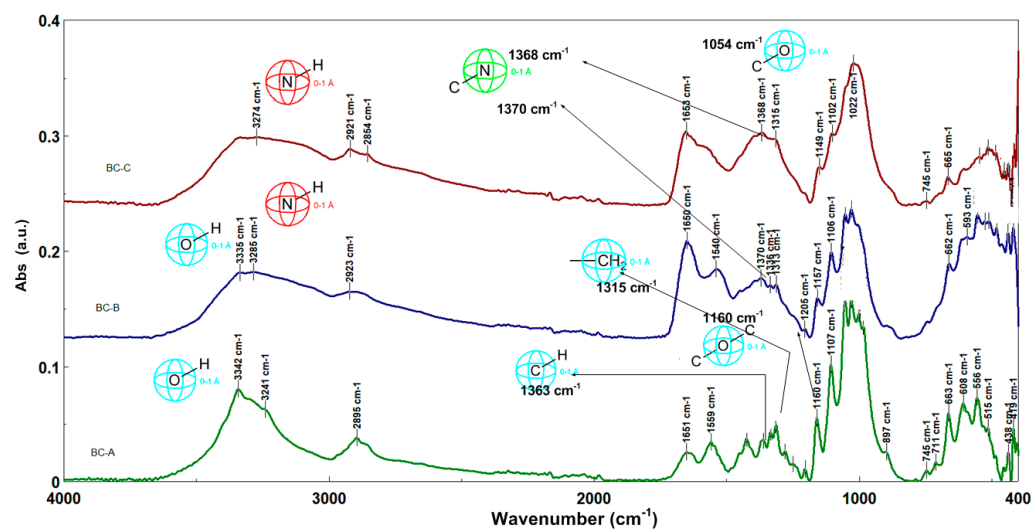

Figure 10. FT-IR summarizing spectra of BC from *Acetobacter* sp. strain: functional groups specific for BC, ($BC_{Gu\text{-}4K}$), and ($BC_{Gu\text{-}48K}$).

2.3. Predicted Responses and Process Factor Optimization

The effects of process factors, i.e., KOH concentration in impregnation solution (*A*), mean surface area of catalyst particle (*B*), agitation speed (*C*), initial alkoxide temperature (*D*), methanol-to-oil molar ratio (*E*), initial oil temperature (*F*), and impregnation time (*G*), on FAME phase yield (Y_{pred}) and soap content in the FAME phase (S_{pred}) were quantified using statistical models described by Equations (1) and (2), where regression coefficients were determined based on experimental data summarized in Table 1 (exp. 1–8). According to Equation (1), higher levels of *F* and lower levels of the other factors lead to higher values of $Y_{pred} = Y$. Equation (2) indicates higher values of $S_{pred} = S$ at higher levels

of *A*, *C*, and *D*, as well as at lower levels of *B*, *E*, *F*, and *G*. Equations (1) and (2) can be used to predict the process responses for values of process factors within ranges considered in the experimental study.

$$Y_{pred} = Y = 103.7 - 163.7A - 0.830B - 0.003C - 0.021D - 0.060E + 0.113F - 0.057G \quad (1)$$

$$S_{pred} = S = 3027 + 7311A - 81.61B + 1.076C + 12.19D - 132.7E - 7.884F - 6.587G \quad (2)$$

Table 1. Levels of process factors and responses.

Exp.	*A* (g/mL)	*B* (cm²)	*C* (rpm)	*D* (°C)	*E* (mol/mol)	*F* (°C)	*G* (h)	*Y* (%)	*S* (ppm)
1	0.053	6.250	300	70	12	70	96	89.08	1303
2	0.053	6.250	0	25	6	25	96	86.32	1583
3	0.053	0.640	300	70	6	25	24	93.12	3386
4	0.053	0.640	0	25	12	70	24	99.81	1364
5	0.027	6.250	300	25	12	25	24	93.32	1394
6	0.027	6.250	0	70	6	70	24	98.81	2061
7	0.027	0.640	300	25	6	70	96	99.31	1819
8	0.027	0.640	0	70	12	25	96	93.92	1603
9	0.027	0.640	0	25	12	70	96	99.91	721.9
10	0.027	0.640	0	25	12	70	96	99.88	704.8
11	0.027	0.640	0	25	12	70	96	99.79	691.4

(*A*) KOH concentration in impregnation solution; (*B*) mean surface area of catalyst particle; (*C*) agitation speed; (*D*) initial alkoxide temperature; (*E*) methanol-to-oil molar ratio; (*F*) initial oil temperature; (*G*) impregnation time; (*Y*) FAME phase yield determined using Equation (4); (*S*) soap content determined using Equation (5).

A desirability function approach was used to determine the optimum factor levels to maximize the FAME phase yield ($Y_{pred} = Y$). A desirability function, $d(Y)$, is defined by Equation (3), where L_Y and U_Y (Figure 11) are the lower and upper limits of response *Y* [25,26]. A completely desirable value of response corresponds to $d(Y) = 1$, whereas $d(Y) = 0$ represents an undesirable value.

$$d(Y) = \begin{cases} 0 & \text{if } Y < L_Y \\ \frac{Y - L_Y}{U_Y - L_Y} & \text{if } L_Y \leq Y \leq U_Y \\ 1 & \text{if } Y > U_Y \end{cases} \quad (3)$$

Profiles for predicted values of *Y* and for desirability function, which are shown in Figure 11, indicate that the optimum values of process factors for maximizing the response *Y* are the low levels of *A*, *B*, *C*, and *D* and high levels of *E*, *F*, and *D* specified in Table 1 (exp. 1–8), as follows: $A_{low} = 0.027$ g/mL, $B_{low} = 0.640$ cm², $C_{low} = 0$ rpm, $D_{low} = 25$ °C, $E_{high} = 12$ mol/mol, $F_{high} = 70$ °C, and $G_{high} = 96$ h. Under these optimum conditions, the process response is $Y_{opt} = 99.96\%$ and desirability function is $d(Y_{opt}) = 1$.

In order to validate the statistical model described by Equation (1), three experimental runs (exp. 9–11 in Table 1) were performed at optimum values of process factors. The difference between the mean value of these replicates ($Y_{mn,opt} = 99.86\%$) and that predicted by Equation (1), i.e., $Y_{opt} = 99.96\%$, is statistically nonsignificant (the modulus of *t*-statistic (−2.75) is lower than its critical value (2.92 for one tail and 4.30 for two tails at a significance level of 0.05)), which demonstrates the model validity. The values of soap content for exp. 9–11, calculated using Equation (2), are also included in Table 1. The difference between the mean value of these replicates and that predicted by Equation (2), i.e., 706.0 ppm and 699.7 ppm, is statistically nonsignificant (*t*-statistic of 0.71 is lower than its critical value), which proves the validity of the statistical model described by Equation (2).
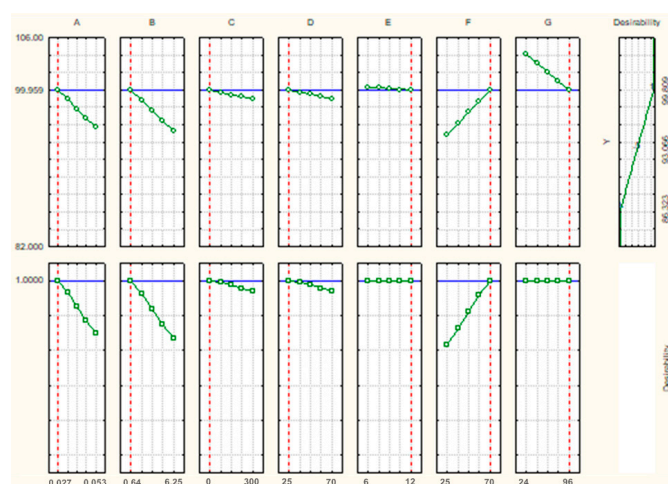
Figure 11. Profiles for predicted values of biodiesel yield ($Y_{pred} = Y$) and related desirability; (*A*) KOH concentration in impregnation solution; (*B*) mean surface area of catalyst particle; (*C*) agitation speed; (*D*) initial alkoxide temperature; (*E*) methanol-to-oil molar ratio; (*F*) initial oil temperature; (*G*) impregnation time.

2.4. Gas Chromatography–Mass Spectrometry (GC-MS) Analysis

GC-MS analysis for alkyl ester identification was carried out for exp. 1 and exp. 8 from present experimental research, and FAME total proportion and chemical composition can be seen in Figures 12 and 13. Figure 12 shows that GC-MS analysis of alkyl esters from exp. 1 led to the identification of 15 different components, with 9,12-octadecadienoic acid (*Z,Z*)-methyl ester as the major component (51.07%), 9-octadecenoic acid methyl ester, (*E*)- as the second major component (38.45%), and hexadecanoic acid methyl ester as the third major component (9.65%). The remaining 12 components were found having under 1% methyl hexadec-9-enoate (0.29%), methyl tetradecanoate (0.22%), linolenic acid methyl ester (0.1), linoleic acid ethyl ester (0.06%), 4-penten-2-ol (0.04%), heptadecanoic acid methyl ester (0.04%), *cis*-10-heptadecenoic acid methyl ester (0.04%), pentadecanoic acid methyl ester (0.03), and octanoic acid methyl ester (0.01%).
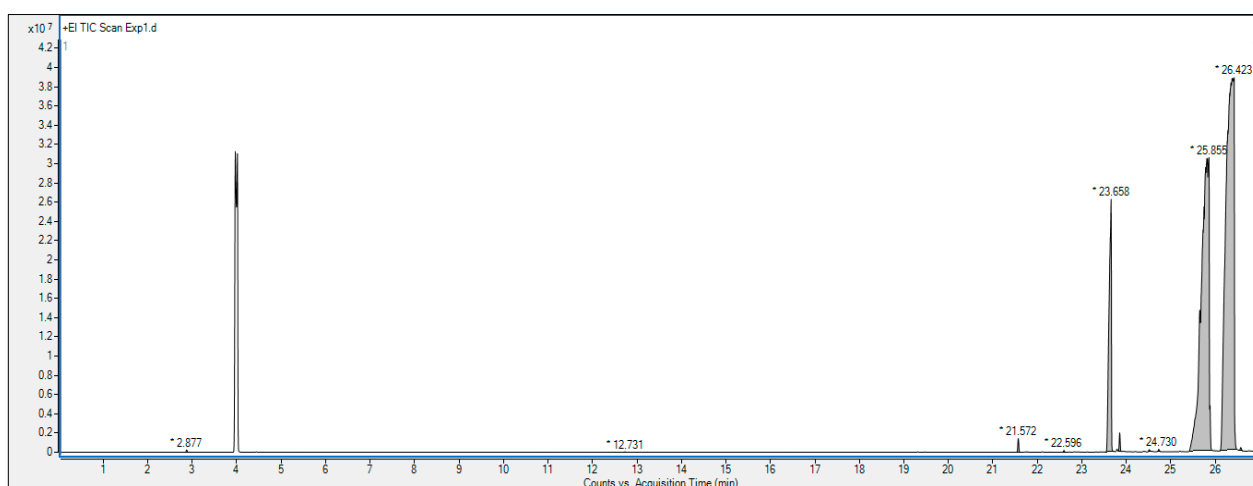

Figure 12. GC-MS analysis for the composition of the alkyl esters in exp. 1.
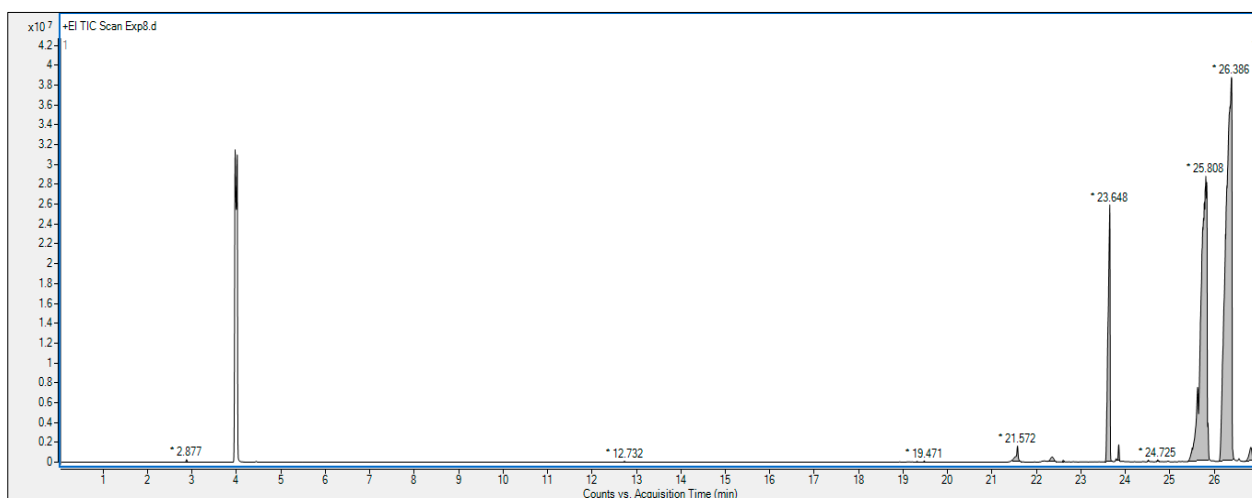
Figure 13. GC-MS analysis for the composition of the alkyl esters in exp. 8.

Figure 13 shows that GC-MS analysis of alkyl esters from exp. 8 led again to the identification of 15 different components, with 9,12-octadecadienoic acid (Z,Z)- methyl ester as the major component (49.44%), 9-octadecenoic acid methyl ester, (*E*)- as the second major component (37.23%), and hexadecanoic acid methyl ester as the third major component (10.95%).

The remaining 12 components were found having under 1% and being slightly different in composition (components and percentage): docosanoic acid methyl ester (0.81%), methyl tetradecanoate (0.67%), palmitoleic acid (0.33%), 9-hexadecenoic acid methyl ester, (Z) (0.30%), 4-penten-2-ol (0.05%), 7-hexadecenoic acid methyl ester, (Z) (0.04%), heptadecanoic acid methyl ester (0.04%), *cis*-10-heptadecenoic acid methyl ester (0.04%), octanoic acid methyl ester (0.03%), methyl 13-methyltetradecanoate (0.03 b%), undecanoic acid, 10-methyl-, methyl ester (0.02%), and 2,4-decadienal (0.02%).

Although they are present in small proportions, rather considerable traces, the presence of docosanoic acid methyl ester, palmitoleic acid (0.33%), 9-hexadecenoic acid methyl ester, (Z), 7-hexadecenoic acid methyl ester, (Z), methyl 13-methyltetradecanoate (0.03 b%), undecanoic acid, 10-methyl-, methyl ester, and 2,4-decadienal provides important data regarding alkyl ester composition, considering these compounds were missing in exp. 1 alkyl ester chemical composition.

3. Materials and Methods

3.1. Materials

Potassium hydroxide pellets (VWR BDH Chemicals, Prague, Czech Republic), methanol 99.9% (Avantor, Gliwice, Poland), guanidine hydrochloride (VWR Chemicals, Radnor, PA, USA), 2-propanol 100% (VWR Chemicals, Paris, France), bromphenol blue (Sigma–Aldrich, Darmstadt, Germany), and waste cooking oil were the materials used in this experimental research.

BC membranes (99% water content) were obtained in static culture from *Acetobacter* sp. strain isolated from traditionally fermented vinegar in the Mass Transfer Laboratory of the Chemical and Biochemical Engineering Department of National University of Sciences and Technologies POLITEHNICA Bucharest [16,27].

3.2. Bacterial Cellulose Production

BC production was performed using a method from previous work [16,27].

Depending on the application, the production time of a BC membrane can be in the range of 7–30 days or even longer. At the daily temperature of 25–30 °C, or at 18–24 °C at night (a temperature considered in the optimal range for the development of BC culture) without thermostating, the period of 7–10 days was sufficient to obtain a BC membrane of

110 mm diameter and of 8 mm thickness [21], which, following post-production treatments, after the drying operation, reached a membrane of 80 mm diameter and of 2.5 mm thickness for a moisture content of 99.4% (experimental). In the present work, the period allocated to the process of obtaining BC was intentionally extended to more than 25 days, resulting in the production of the BC membrane shown in Figure 14b,c.
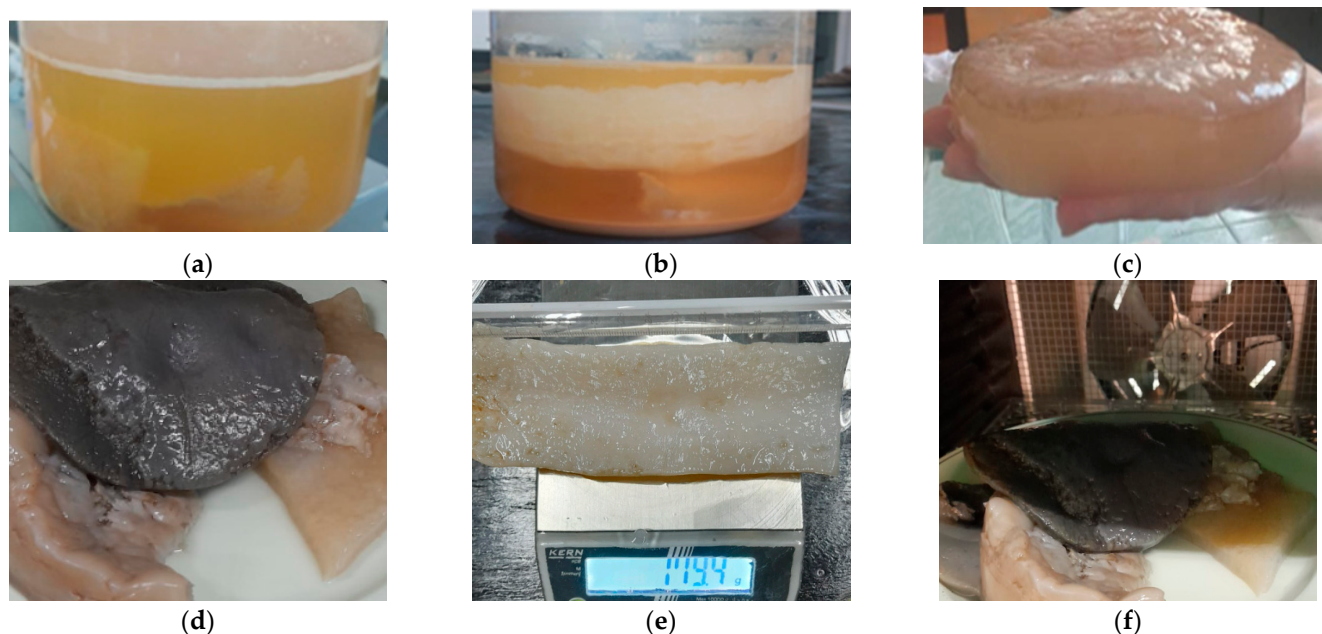

Figure 14. Bacterial cellulose production: (**a**) culture medium, 6 days; (**b**) after 29 days; (**c,d,f**) after weak acid treatment, followed by neutralization; (**e**) under weak acid treatment, ready for functionalization.

After production, the BC can be preserved for a long period of time if kept in a weak acid solution, while its further use involves a fairly standard neutralization method before it is functionalized. For this work, this post-treatment was approached similarly as part of the catalyst construction strategy. After neutralization BC was dried to remove even traces of moisture at 70 °C in a Biovita DEH450 (Figure 14f) dehydrator (voltage of 220–240 V 50 Hz and power of 420–500 W) and then deposited in desiccator. At this stage, this membrane of BC was considered the solid material used for the subsequent functionalization to catalytic support.

Following our strategy developed for the construction of the catalyst, the particles (pieces) of BC of specific dimensions were prepared (Figure 15), after which the impregnation solutions were prepared. These solutions were made in two steps; in the first step, a methanol solution of guanidine hydrochloride and potassium hydroxide of Gu-KOH 1:1 molar ratio was prepared at reflux by heating the reaction mixture under stirring for 6 h at 60 °C and keeping it for 24 h to complete the reaction. In the second stage, the alcoholic guanidine solution (Gu_a) was divided and used for BC functionalization.
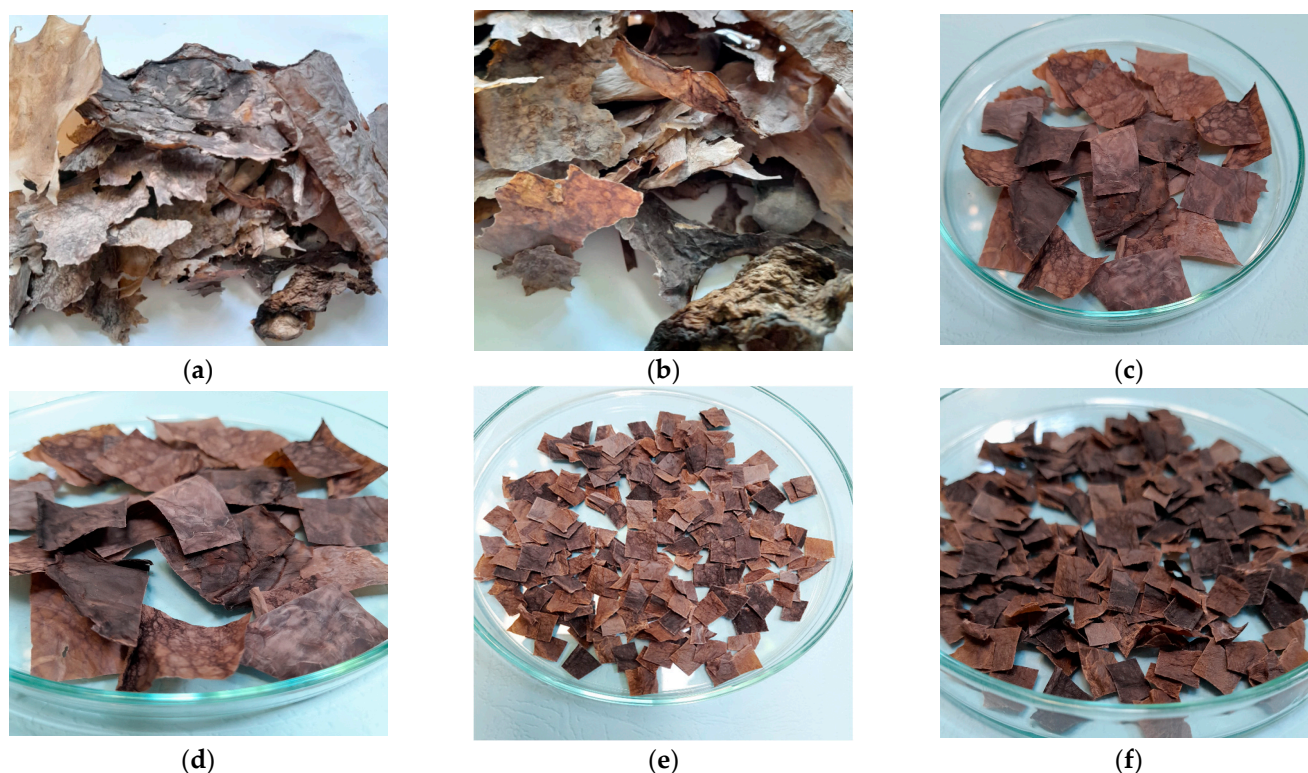
Figure 15. Dried BC: (**a**,**b**) from dehydrator, large dimensions; (**c**,**d**) large pieces according to experimental plan; (**e**,**f**) small particles according to experimental plan.

3.3. Catalyst Preparation

Four Gu_a solutions were later used to prepare the final basic compound for combining with the catalytic support by impregnation: two mixtures for each particle type by adding KOH 1:18.75 w/v to alcoholic guanidine solution (denoted 8K) kept at reflux for 6 h at 60 °C, under stirring, and left for 24 h to complete the reaction and another two different mixtures by adding 1:37.5 w/v KOH in alcoholic guanidine solution (denoted 4K), reacted in a similar way (Table 2), with all four reactions performed in respect with experimental research design. At this point, the catalyst was considered prepared and ready to be tested.

Table 2. *BC* and *BC* catalyst types obtained after functionalization.

Exp.No.	Catalytic Supp./Catalyst	Comments	Observations
1	*BC*	BC, plain, simple	Evaluation
2	*BC$_{Gu}$*	BC in alcoholic guanidine, without KOH	Evaluation
3	*BC$_{Gu-4K24h}$*	BC/superbase (Gu-KOH, 4K, impregnation time 24 h) *	Heterogeneous catalyst
4	*BC$_{Gu-4K96h}$*	BC/superbase (Gu-KOH, 4K, impregnation time 96 h)	Heterogeneous catalyst
5	*BC$_{Gu-8K24h}$*	BC/superbase (Gu-KOH, 8K, impregnation time 24 h) **	Heterogeneous catalyst
6	*BC$_{Gu-4K96h}$*	BC/superbase (Gu-KOH, 8K, impregnation time 96 h)	Heterogeneous catalyst

* KOH 1:18.75 w/v in alcoholic guanidine solution, ** KOH 1:37.5 w/v in alcoholic guanidine solution.

3.4. Catalyst Characterization

Specific analysis was performed for both the characterization of the catalytic support and the heterogeneous catalyst.

3.4.1. Scanning Electron Microscope (SEM) Analysis

The morphology of the guanidine-based catalyst loading in section and on the surface was evaluated using a TM4000Plus Tabletop Scanning Electron Microscope (Hitachi, Tokyo, Japan) at 15 kV in standard vacuum conditions (according to the TM4000Plus Software

vacuum settings). The SEM images were obtained using both backscattered electron (BSE) and/or secondary electron (SE) detectors at multiple magnifications.

3.4.2. Fourier Transform Infrared Spectroscopy

Fourier transform infrared spectroscopy (ATR-FTIR) was performed in the range of 4000–400 cm^{-1} with a Vertex 80 spectrometer (Bruker Optik GMBH, Billerica, MA, USA). An attenuated total reflectance (ATR) accessory was used.

3.5. Catalyst Testing and Analysis

3.5.1. Catalyst Testing in Transesterification Reactions to Alkyl Esters

Testing of the heterogeneous catalyst involved a set of transesterification reactions to alkyl esters under conditions that were specifically selected to be similar to commercial biodiesel production.

3.5.2. Analysis of Main Product in Transesterification Reactions to Alkyl Esters

Alkyl (methyl) ester characterization was performed by gas chromatography–mass spectrometry (GC-MS) analysis using the Agilent 7890 A GC-MS/MS TRIPLE QUAD system. A capillary column Agilent DB-WAX of 30 m length, 0.25 mm internal diameter, and 0.25 μm film thickness was used, having helium at a flow rate of 1 mL/min as the carrier gas. The starting oven temperature was 40 °C; then, a gradual increas up to 210 °C was performed, with an increase of 3 °C/min between 40 and 80 °C, which was kept for 2 min, and then of 15 °C/min up to 210 °C, where it was held again for 2 min. The temperature for GC injector was 250 °C, while the MS detector was set at 150 °C. The temperature for the transfer line was maintained at 280 °C. Electron ionization (EI) mode was used for MS detection, at 70 eV, with a mass scan range of m/z 50–450. The identification of peaks within the analyzed samples was performed according to NIST MS database.

3.5.3. Soap Content in FAME Test Reaction Product

Soap formation during the transesterification reaction to alkyl esters is inevitable [28]. Regardless of whether the methanol is in excess and the reaction is shifted to the desired triesters and regardless of the percentage of FFA reduction or how effectively any traces of water were removed, if you have methanol and NaOH reacting (homogeneous catalyst), you will also have soap. Studies showed, however, that, using heterogeneous catalyst, a lower soap content value can be attained, this being another advantage beside an easier main reaction product separation, thus allowing the alkyl esters to enter the biodiesel standard in this respect. In this context, soap content was determined while testing the catalyst in transesterification reaction in this work.

3.5.4. Independent and Dependent Process Variables

KOH concentration in impregnation solution (*A*), mean surface area of catalyst particle (*B*), agitation speed (*C*), initial alkoxide temperature (*D*), methanol-to-oil molar ratio (*E*), initial oil temperature (*F*), and impregnation time (*G*) were selected as process independent variables (factors). Process dependent variables (responses) were FAME phase yield (*Y*) and final soap content in the FAME phase (*S*), calculated using Equations (4) and (5), where m_{FAME}, m_{oil}, and m_S are the masses of FAME phase, oil, and soap.

$$Y = 100\frac{m_{FAME}}{m_{oil}} \tag{4}$$

$$S = 10^6\frac{m_S}{m_{FAME}} \tag{5}$$

3.5.5. Experimental Design, Statistical Analysis, and Optimization

Experimental design, statistical analysis, and process factor optimization were performed using STATISTICA 10 software (Stat Soft Inc., Tulsa, OK, USA). According to a

Plackett–Burman design, eight experimental runs (1–8 in Table 1) were performed at two levels of process factors.

4. Conclusions

BC used as a catalytic support was able, after impregnation with a guanidine/potassium hydroxide superbase, to heterogeneously catalyze the transesterification of untreated used cooking oil, yielding over 99% methyl esters and, considering the percentage of 96.5% standard biodiesel for its content, it can be said (from this approach alone) that biodiesel is what has been achieved under process conditions similar to those of commercial biodiesel. Further studies and experimental research are needed on the response of BC to different treatments, applied especially after its production and before similar functionalization considering the multitude of variables that need to be addressed in terms of impregnation conditions, targeted chemisorption, or process factors' optimal number of variables.

Author Contributions: Conceptualization, C.I.G., C.E.R., L.E.P., T.D. and O.C.P.; methodology, C.I.G., C.E.R., L.E.P., D.R.C.T., T.D. and O.C.P.; validation, T.D. and O.C.P.; formal analysis, O.C.P.; investigation, C.I.G., C.E.R., L.E.P., D.R.C.T., G.V. and A.L.M.; data curation, D.R.C.T., G.V. and A.L.M.; writing—original draft preparation, C.I.G., C.E.R., L.E.P., D.R.C.T., T.D. and O.C.P.; writing, C.E.R. and O.C.P.; visualization, D.R.C.T., G.V. and A.L.M.; supervision, T.D. and O.C.P. All authors have read and agreed to the published version of the manuscript.

Data Availability Statement: Data is contained within the article.

Conflicts of Interest: The authors declare no conflict of interest.

References

1. Knothe, G.; Van Gerpen, J. Chapter 2—The History of Vegetable Oil-Based Diesel Fuells. In *The Biodiesel Handbook*, 1st ed.; Knothe, G., Van Gerpen, J., Krahl, J., Eds.; AOCS Press Publishing: Champaigne, IL, USA, 2005; pp. 12–24. [CrossRef]
2. Liu, Y.; Boyás, R.S.; Murata, K.; Minowa, T.; Sakanishi, K. Hydrotreatment of vegetable oil to produce bio-hydrogenated diesel and liquefied petroleum gas fuel over catalysts containing sulfided Ni–Mo and solid acids. *Energy Fuel* **2011**, *25*, 4675–4685. [CrossRef]
3. Murata, K.; Liu, Y.; Inaba, M.; Takahara, I. Production of synthetic diesel by hydrotreatment of Jatropha oils using Pt–Re/H-ZSM-5 catalyst. *Energy Fuel* **2010**, *24*, 2404–2409. [CrossRef]
4. Veriansyah, B.; Han, J.Y.; Kim, S.K.; Hong, S.A.; Kim, Y.J.; Lim, J.S.; Shu, Y.W.; Oh, S.G.; Kim, J. Production of renewable diesel by hydroprocessing of soybean oil: Effect of catalysts. *Fuel* **2011**, *94*, 578–585. [CrossRef]
5. Hydrotreating Catalysts and Technologies for All Crude Oil Fractions. Available online: http://www.topsoe.com/processes/hydrotreating (accessed on 30 September 2023).
6. Demirbas, A.; Bafail, A.; Ahmad, W.; Sheikh, M. Biodiesel production from non-edible plant oils. *Energy Explor. Exploit.* **2016**, *34*, 290–318. [CrossRef]
7. Castro, E.; Strætkvern, K.O.; Romero-García, J.M.; Martín, C. Pretreatment and Bioconversion for Valorization of Residues of Non-Edible Oilseeds. *Agronomy* **2023**, *13*, 2196. [CrossRef]
8. Neto, J.M.; Komesu, A.; Da Silva Martins, L.H.; Gonçalves, V.O.O.; De Oliveira, J.A.R.; Rai, M.; Ingle, A.P. Chapter 10—Third generation biofuels: An overview. In *Sustainable Bioenerg*; Rai, M., Ingle, A.P., Eds.; Elsevier: Amsterdam, The Netherlands, 2019; pp. 283–298. [CrossRef]
9. Bhatia, K.S.; Gurav, R.; Choi, T.R.; Kim, H.J.; Yang, S.Y.; Hong, H.S.; Park, J.Y.; Park, Y.L.; Han, Y.H.; Choi, Y.K.; et al. Conversion of waste cooking oil into biodiesel using heterogenous catalyst derived from cork biochar. *Bioresour. Technol.* **2020**, *302*, 122872. [CrossRef]
10. Singh, H.; Ali, A. Esterification as well as transesterification of waste oil using potassium imbued tungstophosphoric acid supported graphene oxide as heterogeneous catalyst: Optimization and kinetic modeling. *Renew. Energy* **2023**, *207*, 422–435. [CrossRef]

11. Chinglenthoiba, C.; Das, A.; Vandana, S. Enhanced biodiesel production from waste cooking palm oil, with NaOH-loaded Calcined fish bones as the catalyst. *Environ. Sci. Pollut. Res.* **2020**, *27*, 15925–15930. [CrossRef]

12. Poddar, M.K.; Pritam Kumar Dikshit, P.K. Recent development in bacterial cellulose production and synthesis of cellulose based conductive polymer nanocomposites. *Nano Select* **2021**, *2*, 1605–1628. [CrossRef]

13. Sharma, P.; Mittal, M.; Yadav, A.; Aggarwal, N.K. Bacterial cellulose: Nano-biomaterial for biodegradable face masks—A greener approach towards environment. *Environ. Nanotechnol. Monit. Manag.* **2023**, *19*, 100759. [CrossRef] [PubMed]

14. Bueno, F.; Fultz, L.; Husseneder, C.; Keenan, M.; Sathivel, S. Biodegradability of bacterial cellulose polymer below the soil and its effects on soil bacteria diversity. *Polym. Degrad. Stab.* **2023**, *217*, 110535. [CrossRef]

15. Fernando, G.; Torres, F.G.; Solene Commeaux, S.; Omar, P.; Troncoso, O.P. Biocompatibility of Bacterial Cellulose Based Biomaterials. *J. Funct. Biomater.* **2012**, *3*, 864–878. [CrossRef]

16. Păvăloiu, R.D.; Stroescu, M.; Pârvulescu, O.C.; Dobre, T. Composite hydrogels of bacterial cellulose-carboxymethyl cellulose for drug release. *Rev. Chim.* **2014**, *65*, 948–951.

17. Parvulescu, O.P.; Isopencu, G.; Busuioc, C.; Raducanu, C.; Mocanu, A.; Deleanu, I.; Stoica-Guzun, A. Chapter 17—Antimicrobial bacterial cellulose composites as textile materials. In *Antimicrobial Textiles from Natural Resources*; Mondal, I.H., Ed.; Woodhead Publishing: Sawston, UK, 2021; pp. 513–556. [CrossRef]

18. Dai, Q.; Liu, J.; Zheng, J.; Fu, B. Immobilization of UiO-66-NH2 into Bacterial Cellulose Aerogels for Efficient Particulate Matter Filtration. *Sustainability* **2023**, *15*, 13382. [CrossRef]

19. Tahir, D.; Karim, M.R.A.; Hu, H.; Naseem, S.; Rehan, M.; Ahmad, M.; Zhang, M. Sources, Chemical Functionalization, and Commercial Applications of Nanocellulose and Nanocellulose Based Composites: A Review. *Polymers* **2022**, *14*, 4468. [CrossRef] [PubMed]

20. Wahab, R.M.A.E.; Ghanem, A.F.; Sheir, D.H.; Selim, M.M.; Zaher, F.A.; Badawy, A.A. Assessment of a green zeolite/bacterial cellulose nanocomposite membrane as a catalyst to produce biodiesel from waste cooking oil. *Energy Sources Part A Recovery Util. Environ. Eff.* **2023**, *45*, 10350–10365. [CrossRef]

21. Raducanu, C.E. New Solutions Regarding Catalytic Transesterification Integration with Separation in Biodiesel Technology. Ph.D. Thesis, Chemical and Biochemical Engineering Department, Faculty of Chemical Engineering and Biotechnologies, National University of Sciences and Technologies POLITEHNICA Bucharest, Bucharest, Romania, 2020.

22. Drozd, M.; Dudzic, D.; Pietraszko, A. Crystal structure, differential scanning calorimetric, infrared spectroscopy and theoretical studies of C(NH2)2(NH)CH2@CHCOOH noncentrosymmetric crystal. *Spectrochim. Acta Part A Mol. Biomol. Spectrosc.* **2013**, *105*, 135–148. [CrossRef]

23. Haynes, W.M.; Lide, D.R.; Bruno, T.J. Chapter 8—Analytical Chemistry. In *Handbook of chemistry and Physics: A Ready-Reference Book of Chemical and Physical Data*, 97th ed.; CRC Press: Boca Raton, FL, USA, 2016; Volume 1, pp. 43–48.

24. Nelli Atykyan, N.; Victor Revin, V.; Shutova, V. Raman and FT-IR Spectroscopy investigation the cellulose structural differences from bacteria Gluconacetobacter sucrofermentans during the different regimes of cultivation on a molasses media. *AMB Express* **2020**, *10*, 84. [CrossRef]

25. Dima, A.D.; Pârvulescu, O.C.; Mateescu, C.; Dobre, T. Optimization of substrate composition in anaerobic co-digestion of agricultural waste using central composite design. *Biomass Bioenerg.* **2020**, *138*, 105602. [CrossRef]

26. Drăghici-Popa, A.-M.; Boscornea, A.C.; Brezoiu, A.-M.; Tomas, S.T.; Pârvulescu, O.C.; Stan, R. Effects of extraction process factors on the composition and antioxidant activity of blackthorn (*Prunus spinosa* L.) fruit extracts. *Antioxidants* **2023**, *12*, 1897. [CrossRef]

27. Dobre, T.; Stoica, A.; Pârvulescu, O.C.; Stroescu, M.; Iavorschi, G. Factors influence on bacterial cellulose growth in static reactors. *Rev. Chim.* **2008**, *59*, 591–594. [CrossRef]

28. Chanakaewsomboon, I.; Tongurai, C.; Photaworn, S.; Kungsanant, S.; Nikhom, R. Investigation of saponification mechanisms in biodiesel production: Microscopic visualization of the effects of FFA, water and the amount of alkaline catalyst. *J. Environ. Chem. Eng.* **2020**, *8*, 103538. [CrossRef]